applied sciences

MDPI

Article

A Novel Focal Length Measurement Method for Center-Obstructed Omni-Directional Reflective Optical Systems

Hojong Choi [1], Joo-Youn Jo [2] and Jae-Myung Ryu [2,*]

1 Department of Medical IT Convergence Engineering, Kumoh National Institute of Technology, Gumi-si 39253, Korea; hojongch@kumoh.ac.kr

2 Department of Optical Engineering, Kumoh National Institute of Technology, Gumi-si 39253, Korea; jojooyoun7@naver.com

* Correspondence: jmryu@kumoh.ac.kr; Tel.: +82-54-478-7778

Received: 22 May 2019; Accepted: 5 June 2019; Published: 8 June 2019

Abstract: An omni-directional optical system can be used as a surveillance camera owing to its wide field angle. In cases in which a system is designed with a central screen obscuring structure to increase the resolution of the off-axis field, however, the conventional methods cannot be used to measure the effective focal length (EFL). We assumed the actual and theoretical distortion values of the fabricated optical system to be the same and determined the system's EFL by finding the minimum deviation point of the measured and theoretical distortions. The feasibility of the determined EFL was verified through a tolerance analysis of the system. For these precise measurements we also analyzed the sources of error. To verify our proposed measurement method, we measured the focal length of a center-obstructed omni-directional reflective optical system with an 80–135° field of view (FOV). The EFL from the measurement was 0.3739 mm and was only approximately 11 µm different from the EFL calculated using the design software. Thus, the reliability of focal length measurements in omni-directional optical systems was improved.

Keywords: omni-directional reflective optical system; focal length measurement; geometrical optics; optical design; tolerance analysis

1. Introduction

The 9/11 terrorist attack in New York in 2001 has led to tremendous growth in security-related markets. Most of the key security products that employ optical design technology (e.g., fingerprint identification systems and cameras) are used for building security [1]. These devices capture optical images of people approaching a building to help identify possible intruders among numerous visitors [2]. These cameras often use a zoom lens because normal monitoring is performed in wide mode and zooming allows a person or an object to be observed in tele mode by changing the field of view (FOV) [1]. However, a zoom lens not only has a limited FOV, but also requires mechanical movement if the need-to-be recognized target is beyond its FOV [3,4]. In such cases, security may be compromised if the target approaches swiftly while the camera is moving. To overcome this weakness, an optical system with an FOV of 180° must be used to monitor a wide FOV range with no mechanical movement. Unfortunately, a system with an FOV of 180° or greater does not usually provide satisfactory resolution because the increase in FOV leads to a sharp rise in aberrations such as coma, astigmatism, and field curvature, all of which affect the image quality of the off-axis field [5]. Due to this resolution degradation, a clear image cannot be obtained, nor can the target be accurately recognized even with a high-pixel image sensor [6]. An optical system with a higher off-axis resolution can be designed to overcome this issue by obstructing the center while giving more weight to the off-axis area than the center [7].

If the FOV of a system is increased to greater than 180° and positioned vertically, a 360° wide view perpendicular to the optical axis is possible. This optical system is called an omni-directional optical system [8]. Despite its center being obstructed, there is no functional issue because the screen center is facing the sky. Meanwhile, the system's effective focal length (EFL), the key physical parameter of an optical system, must be measured to determine the modulation transfer function, distortion, etc. There are four official EFL measurement methods [9] and of these, the nodal slide and magnification methods are the most frequently used. Another method is to use an object at a very far distance to extrapolate data. However, the principles of this method are similar to those of the abovementioned nodal slide and magnification methods. Moreover, these two methods are rarely used in practice [9]. The nodal slide method is based on the principle that chart images never move when a system rotates on its nodal point. Once the nodal point is located, the EFL can be determined. The magnification method, in contrast, uses a chart of known size and a collimator of known focal length to calculate the EFL, using the imaging magnification of the chart that is obtained from the image when the chart passes through the collimator and the test optical system [9]. These methods are characterized by the use of the paraxial property near the screen center, which cannot be applied to a center-obstructed omni-directional optical system. This study investigates a method for measuring the EFL of a center-obstructed omni-directional optical system.

2. Materials and Methods

2.1. Theory

As mentioned in Section 1, the nodal slide or magnification methods are generally used to measure the EFL of an optical system [9]. Figure 1 shows the layout of the focal length measurement system using a nodal bench.

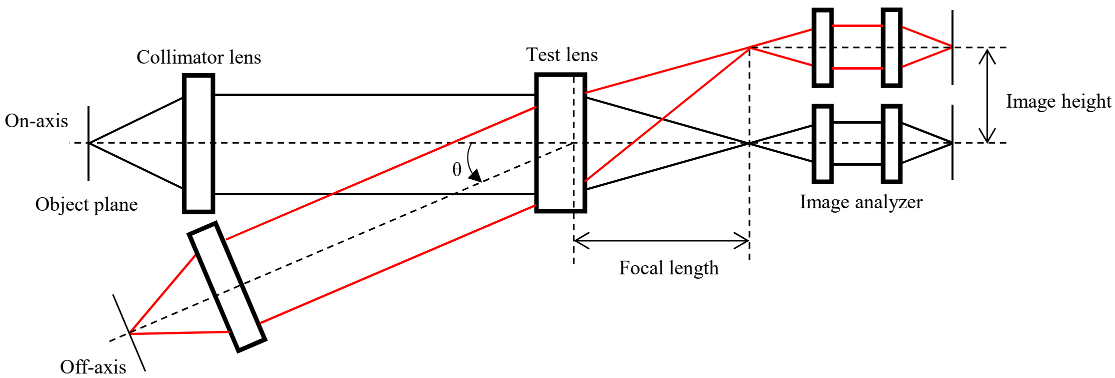

Figure 1. Layout of the focal length and distortion measurement system.

As shown in Figure 1, the measurement system is composed of a collimator, which converts light from a light source into a collimated beam, a test lens to be measured, and an image analyzer, which magnifies the image formed by the test lens [10]. In other words, light starts as a pattern from an object plane illuminated by a light source and is converted into a collimated beam by the collimator lens. The collimated beam then passes through the test lens to form an image and, finally, an image analyzer magnifies the image to ascertain the exact image position. Here, if the sizes of the object plane pattern and the image formed by the test lens are known, we can determine the image magnification of the system equipped with a collimator and the test lens. In addition, if the EFL of the collimator is correctly known, we can find the EFL of the test lens [11].

Next, we move the image analyzer laterally to find the image formed by the test lens after an off-axis beam is incident on the test lens as the collimator rotates. Using the EFL of the test lens obtained earlier and the rotation angle of the collimator, the paraxial image height can be calculated, unless there is distortion by the test lens [12]. The deviation between the calculated paraxial image height and the measured moving distance of the image analyzer becomes a distortion and is described by the following equation [13]:

$$DIY_{real} = \frac{y_{T_i} - f \cdot \tan\theta_i}{f \cdot \tan\theta_i} \tag{1}$$

where f and θ are the EFL of the test lens and the rotation angle of the collimator, respectively. And y_{T_i} is the chief ray height measured as the moving distance of the image analyzer. And the subscript i stands for the number of the data measurement.

Due to the obstruction of the central area in an omni-directional system, the image magnification of systems with a collimator and the test lens cannot be measured using a designed measurement system, such as the one depicted in Figure 1. In addition to this image magnification measurement, an alternative method of measurement entails rotating the test lens imperceptibly about its nodal point. However, this method can be used only if the image is formed near the center of the screen. For this reason, it would be impossible to measure the EFL of a center-obstructed test lens using the layout shown in Figure 1.

If the EFL for the layout shown in Figure 1 is not given, it is worth considering the use of Equation (1) to determine the EFL. y_{T_i} in Equation (1) refers to the chief ray height for the i-th incidence angle. Let us assume here that the design value obtained from the optical design software is used for the distortion by the incident angle in testing the omni-directional system. By representing the distortion calculated using the optical design software as DIY_i and the distortion calculated by Equation (1) as DIY_{real}, we can calculate the sum of squares of deviation for these two distortions (ϕ) using the following equation:

$$\phi = \sum_{i=1}^{n} (DIY_{real} - DIY_i)^2 = \sum_{i=1}^{n} \left(\frac{y_{T_i} - f \cdot \tan\theta_i}{f \cdot \tan\theta_i} - DIY_i \right)^2. \tag{2}$$

The only unknown value in Equation (2) is f, which is the EFL of the optical system. By differentiating Equation (2) with respect to f we obtain the following equation:

$$\frac{d\phi}{df} = \sum_{i=1}^{n} \left\{ \frac{2y_{T_i}}{f^3 \tan\theta_i} \left(f + f \cdot DIY_i - \frac{y_{T_i}}{\tan\theta_i} \right) \right\} = \frac{2}{f^3} \sum_{i=1}^{n} \left\{ f \cdot \frac{y_{T_i}(1 + DIY_i)}{\tan\theta_i} - \frac{y_{T_i}^2}{\tan^2\theta_i} \right\}. \tag{3}$$

By summarizing Equation (3) with respect to f, a condition satisfying the minimum of Equation (2) can be obtained, and the deviation between the theoretical distortion and the measured distortion becomes the minimum. This condition is given by:

$$f = \frac{\sum_{i=1}^{n} \left(\frac{y_{T_i}^2}{\tan^2\theta_i} \right)}{\sum_{i=1}^{n} \left(\frac{y_{T_i}}{\tan\theta_i} - \frac{y_{T_i} \cdot DIY_i}{\tan\theta_i} \right)}. \tag{4}$$

2.2. Measuring the System Configuration

To calculate the EFL using Equation (3), one must know the image height (y_{T_i}), the FOV of θ calculated from the object height, and the theoretical distortion of DIY_i calculated using the optical design software. In other words, the FOV of θ and y_{T_i} should be calculated using Equation (3). For the layout shown in Figure 1, the travel distance of the image analyzer of y_{T_i} can be measured by rotating the collimator or test lens by θ. Unfortunately, this method not only requires a precise collimator and an image analyzer, but also a rotation guide to rotate the test lens or collimator and a linear guide to move the image analyzer, which are extremely expensive. The purpose of this study, therefore, is to use an affordable method to measure the focal length of an omni-directional system.

Figure 2 shows the layout for the method used in this study; the illustration in the upper right of Figure 2 depicts the optical layout of the system to be measured in this study. The pattern in Figure 2 is designed to be equally spaced. Y_T, Y_B, Y_p, and X refer to the overall height of the pattern, the height from the floor surface to the reference plane, the height from the reference plane to the top of the pattern, and the distance between the optical axis and the pattern, respectively. Here, the reference plane is perpendicular to the FOV, which includes the chief ray. A ray reflected from the pattern is captured on the image sensor by the omni-directional system. We can obtain the image height for each position of the pattern as well as the angle θ incident on the optical system from the configuration in Figure 2. The angle of the ray, θ, can be evaluated using the position of each pattern and the distance between the pattern and the optical system.

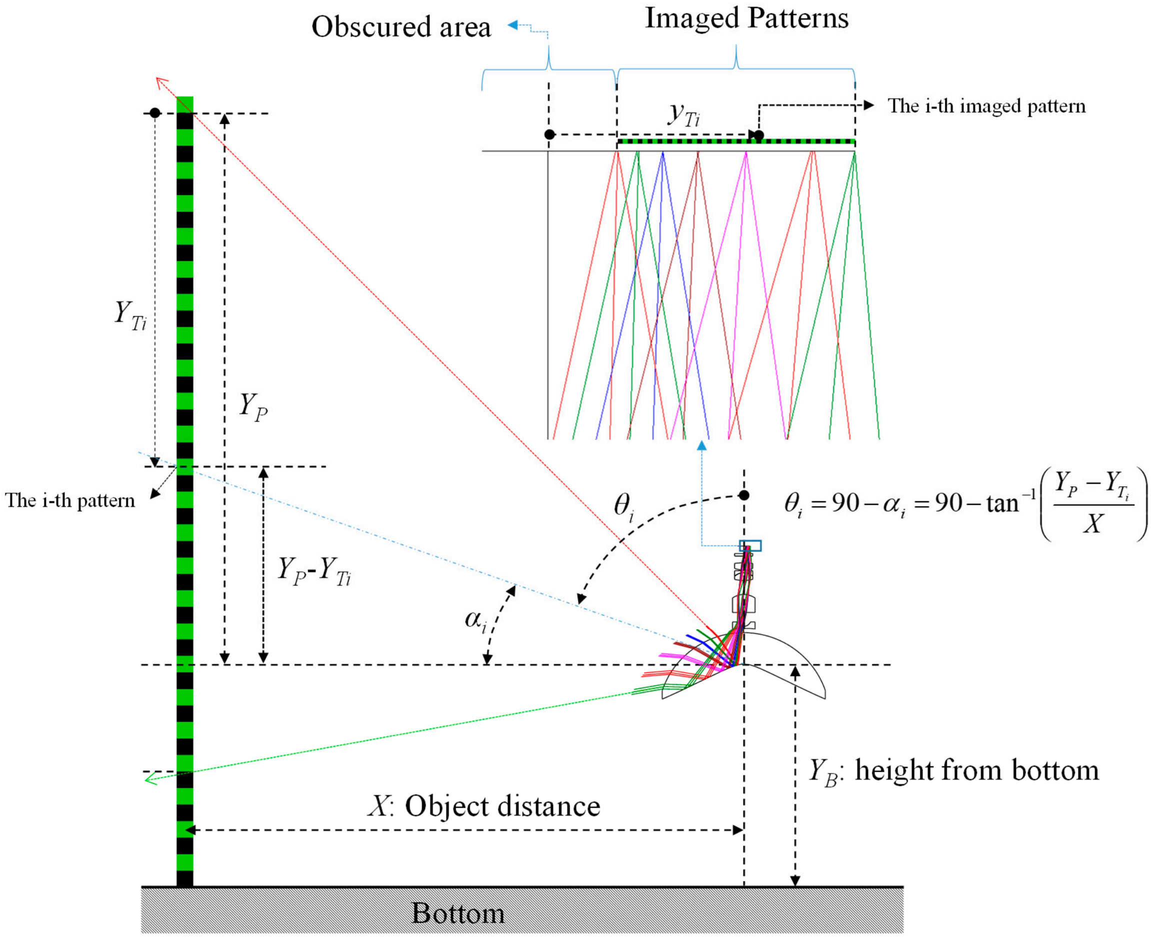

Figure 2. Layout of the measurement system.

Figure 3 shows a photograph taken during an experiment performed using the setup shown in Figure 2. The distance from the optical system to the pattern is designed to be longer than the hyperfocal distance. By doing this, we can prevent the degradation of image quality due to defocusing. This also allows us to ignore the magnification changes induced by the pattern height. As a result, the measurement error in the image height can be minimized. The distance to the pattern (X) and the pattern width were chosen such that the image for each pattern was distinguishable in pixels in the measured images. In addition, the four patterns were placed 90° apart, as shown in Figure 3, to ascertain the variation in the EFL with respect to the position around the optical system.

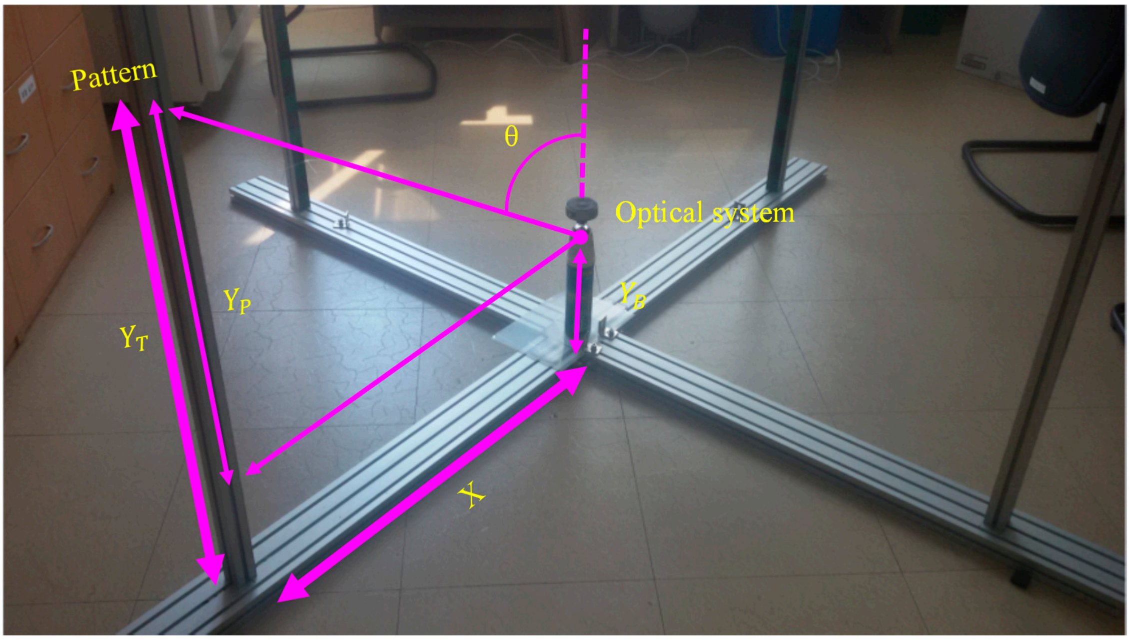

Figure 3. Photograph of the measurement system.

3. Results

3.1. Measurement Analysis and Focal Length Calculation

The specifications of the optical system used in this study are given in Table S1. Six lenses were used in this system. The first lens has a reflective surface on its back. The first lens plays the role of a converter, converting the wide field angle of an item to a narrow field angle. The optical system beyond the second lens is of the retro-focus type, and forms an image of a ray passing through the first lens on the image sensor.

Figure 4 shows the pattern images taken with the system. The patterns were installed 90° apart, as shown in Figure 3, and there are four patterns in the image, as shown in Figure 4. The omni-directional system is generally designed to have the maximum FOV at the shorter side of the image sensor. Thus, the image obtained at the image sensor has the same number of vertical and horizontal pixels, as shown in Figure 4. The calculation of the number of pixels in the pattern helps determine Y_T using Equation (1). The incident angle, θ, for the pattern can also be easily determined owing to the uniformity of the pattern. For an accurate calculation of Y_T, however, we need to identify the screen center. The center of the image sensor and that of the optical system may not coincide due to assembly error within the system and the image sensor. Figure 5, an enlarged image of the central obscuration in Figure 4, shows a photograph of the screen center obtained from an extension line of the pattern shown in Figure 4. The center of the screen obtained using this method would be at 744 pixels crosswise and 807 pixels lengthwise from the upper left of the screen.

Figure 6 shows an enlarged image of Point 1 in Figure 4. We used Adobe Photoshop (Adobe Photoshop 2016, Adobe Systems, San Jose, CA, USA) to determine the pattern's cutoff point. The pattern has alternating black and green rectangles of the same size; hence, we can calculate the pattern height at the edge point where the "G" (green) value of the pixel information changes rapidly, as shown in Figure 6. The pattern height here would be y_{T_i} in Equation (1).

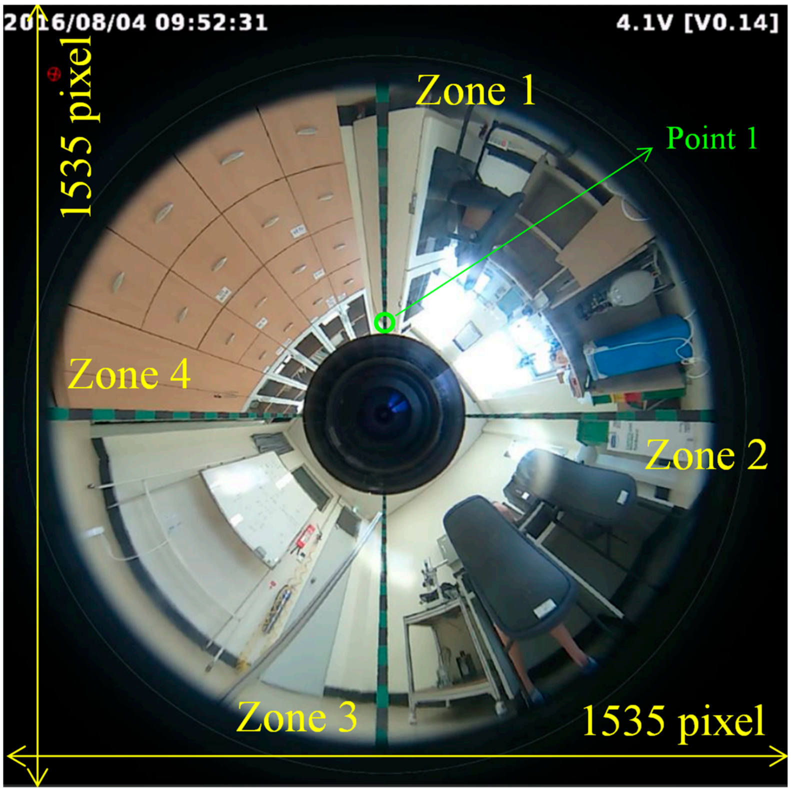

Figure 4. Recorded image.

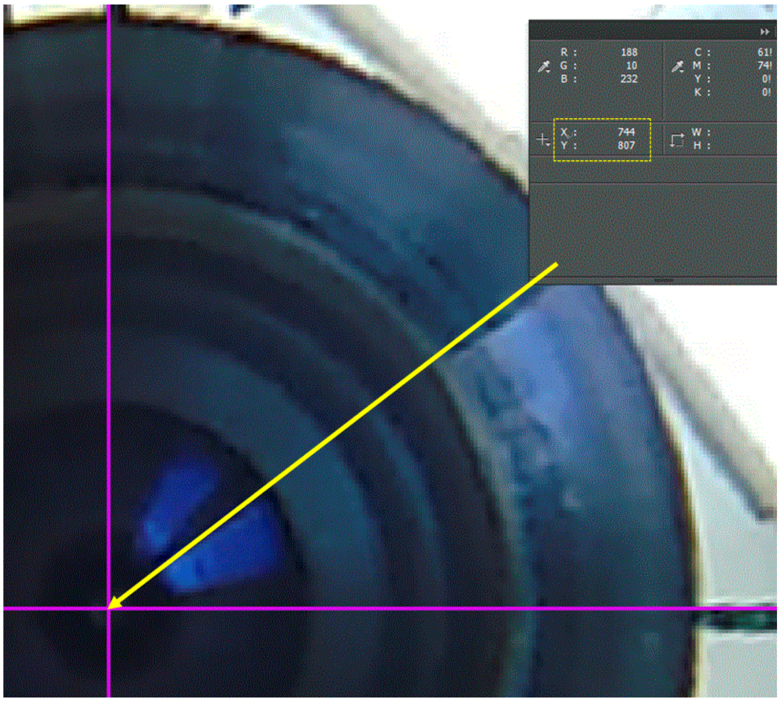

Figure 5. Enlarged image in Photoshop.

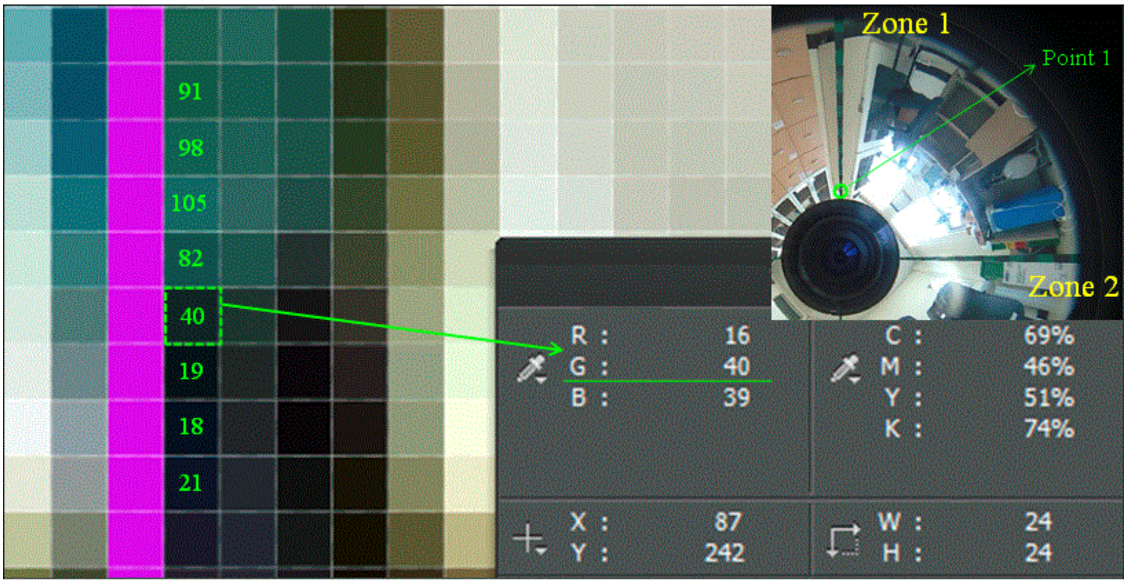

Figure 6. Enlarged image at Point 1 in Figure 4.

Table S2 lists the calculated pattern heights (Y_T) for the pixel sizes given in Table S1 obtained after calculating Y_T for the pixels at the edges of the pattern. Table S3 lists the pattern heights used to obtain θ, the FOV of the ray incident on the optical system. X, Y_T, and Y_B in Table S3 refer to the distance from the center of the system to the point where the pattern is measured, the height from the bottom of the pattern to the particular pattern shape, and the height from the base to the optical system, respectively. Yp is the difference between Y_T and Y_B, from which θ can be calculated. *DIY* is the distortion calculated from each θ value with the optical system software (Code V, Synopsys, Santa Clara, CA, USA). The Y_T values in Table S3 are the mean values of those presented in Table S2.

All the variables required to calculate the EFL are thus compiled and the EFL can be calculated by substituting the values from Table S3 into Equation (3). Table S4 lists the EFL values calculated from the FOV (θ) and the distortion (*DIY*) in Table S3 and Y_T in Table S2 for the images of four identical patterns. In addition, Figure 7 shows a histogram of the EFLs calculated from the measurements tabulated in Table S4. The average EFL is 0.3739 mm. The calculated EFL is slightly greater than the theoretical value, as can be seen in Figure 7.

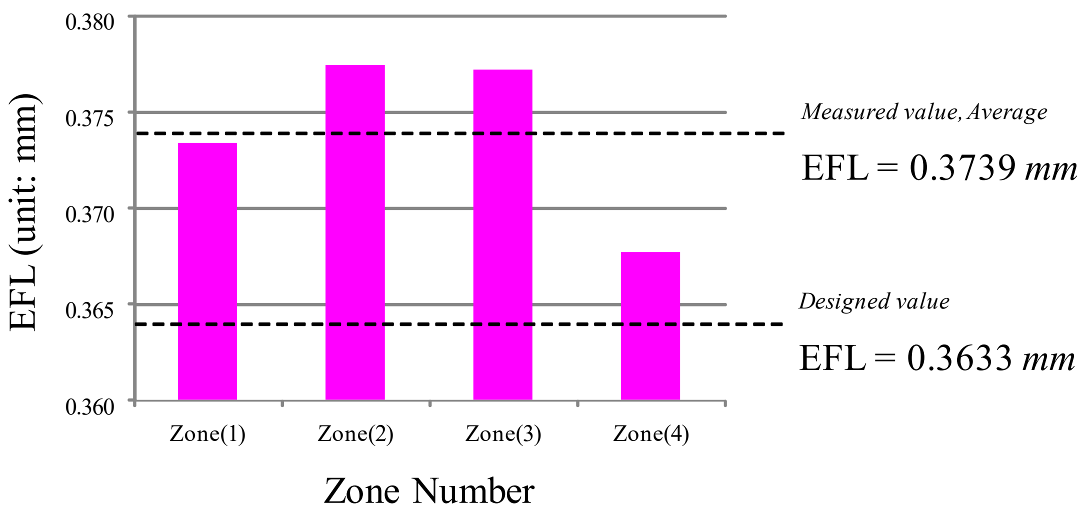

Figure 7. Histogram of the measured EFLs.

3.2. Error Analysis

It is necessary to verify the validity of the calculated EFLs in Table S4, as well as the level of measurement precision. Manufacturing and assembly errors are inevitable when parts are mass-produced. Thus, errors within the limit of the performance boundary of the product are allowed, in general, and such allowed errors are referred to as the tolerance [14,15]. The validity of the measurement method used in this study was verified by checking whether the measured EFL fell within the tolerance range [16]. The EFL of a system can be expressed as a function of the curvature (R), thickness (d), and refractive index (n) of the lens material as follows:

$$EFL = f(R_1, d_1, n_1, R_2, d_2, n_2, R_3, \cdots, R_i, d_i, n_i) \tag{5}$$

where the subscript I stands for the surface number.

Re-expressing Equation (5) using a Taylor series to identify the infinitesimal changes in the function for each tolerance item gives:

$$EFL = EFL_0 + \frac{\partial f}{\partial R}\Delta R_1 + \frac{\partial f}{\partial d}\Delta d_1 + \frac{\partial f}{\partial n}\Delta n_1 + \cdots \tag{6}$$

where EFL_0 is the initial value of the focal length and ΔR,Δd, and Δn refer to errors in the radius of the curvature, thickness, and refractive index, respectively. In this case, only the first-order term needs to be considered because the higher-order terms give little contribution [17]. The coefficients of the errors in the radius of the curvature, thickness, and refractive index in Equation (5) are calculated by differentiating Equation (5). Equation (5) is not analytic, however, and the coefficients of Equation (6) must be calculated by entering the EFL change for the given tolerance into the optical design software. Table S5 lists the EFL sensitivities calculated for a typical tolerance error of an optical system.

If the standard deviations of the curvature, thickness, and refractive index follow a normal distribution of the tolerance error, the standard deviation for the overall changes in the EFL (f) for the system may be calculated by summing the squares of each design variable's standard deviation. This is because the change in the EFL of the system is expressible as a linear sum of the EFL changes in relation to the errors in each design variable, as shown in Equation (6). Moreover, the standard deviations would be larger if the statistical distribution of each design variable did not follow a normal distribution, but instead followed a triangular or a uniform distribution. Even if the errors are not normally distributed, as long as there are plentiful sample data within the distribution, the standard deviation for the EFL changes may be interpreted equally as the normal distribution based on the central limit theorem [18]. The standard deviation of the triangular distribution with poor error management and that of the uniform distribution, at worst, can be approximately calculated as $\sqrt{2}$–$\sqrt{3}$ greater than the standard deviation of the normal distribution [19]. Table S6 lists the calculated standard deviations of the statistical distribution of the design variables when they follow triangular, uniform, and normal distributions.

Under the assumption that each design variable is normally distributed, the standard deviation for the distribution of EFL changes in the optical system calculated from Table S5 would be ~4.84 μm. Thus, the difference between the measured and theoretical EFL is a factor of ~2.2. Moreover, there is a 99.7% probability that the EFL would be distributed within a factor of 3 of the standard deviation because the EFL changes are normally distributed. The statistical distribution of the Newton ring, which indicates the error of curvature at the lens manufacturing stage, and the thickness are prone to be shifted towards a greater mean value [20,21]. The EFL distribution of the manufactured optical system would be shifted slightly more than the design value. Therefore, the measured EFL in this study may be regarded as a valid measurement.

For practical uses of this study, the accuracy of the measurements must be verified. Here, we discuss the possible sources of error during the EFL measurement and methods to improve this measurement. Figure 8 shows the magnified optical paths of the optical system near the first and second lenses. The height from the floor surface to the reference plane changes with changes in the incident angle of the optical system, as shown in Figure 8. This is the first source of error. Because the calculations performed with the measurements, tabulated in Table S3, used the same Y_B on the assumption that the reference point is the same in all cases, there was error in the height from the reference plane to the pattern, Y_p, which caused error in the measured angles. In order to use Y_B in this calculation instead of the approximation, rays would need to be traced using the system simulation and the height would need to be calculated for each pattern. Since the angle of the pattern and the distance away from the center are set to the same value in the simulation, it would be very difficult to calculate the height corresponding to every ray. Another method for using an approximation of Y_B, but with less error compared to the previous method, would be to increase X, the distance between the optical system and the pattern. If X is greater than that used in the previous measurement, Y_T also increases when the same field angle is measured. Because the pattern height, Y_p, is the difference between Y_T and Y_B, the effect of Y_B on the calculation error of Y_p decreases as Y_T increases, thus reducing the error in the angle calculation.

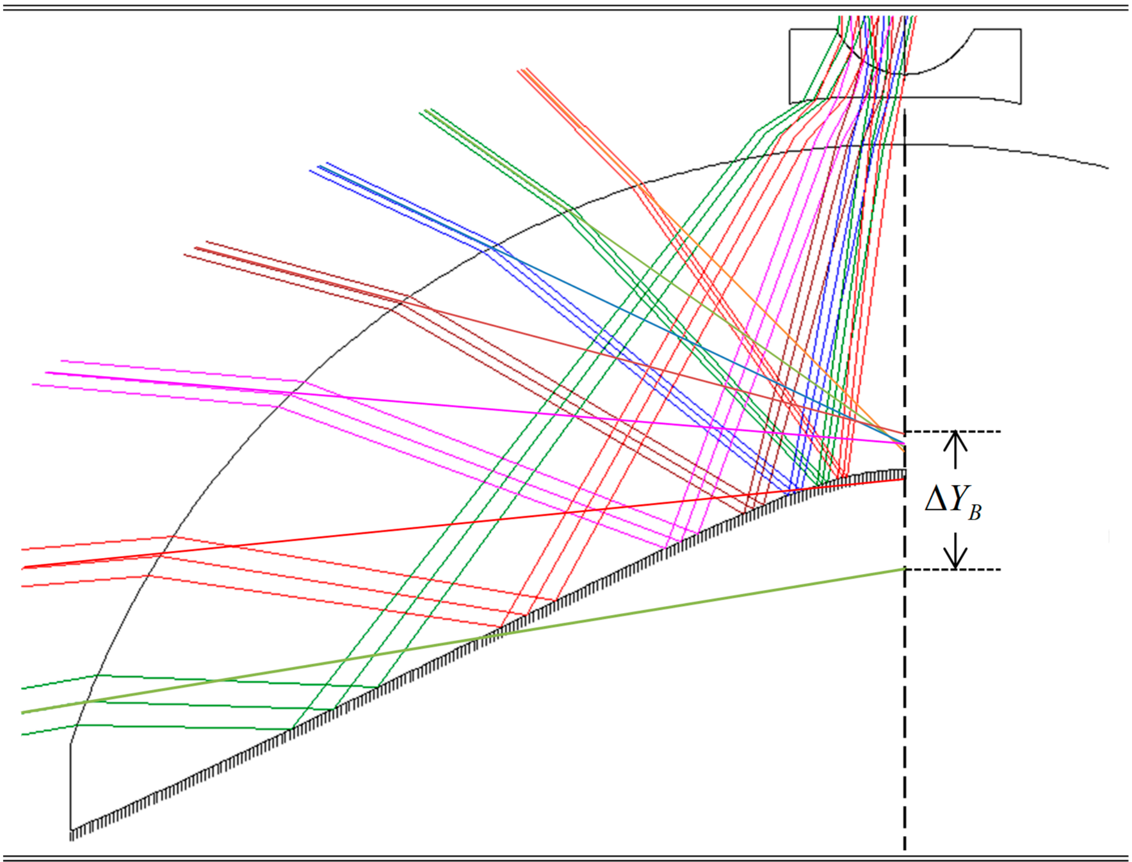

Figure 8. Optical paths of the various rays in the omni-directional reflective optical system.

The second source of error is the inaccurate recognition of pixels. The reference for determining the cutoff point of a pattern in Figure 6 is the sudden change of the color component in a pixel. The "G" (green) color component is the only one needed because the pattern used in this study has green patterns on a black background. The accuracy of pattern recognition may be enhanced by providing clear contrast in the pattern shape. The third source of error is the tilt error between the measurable optical system and the pattern. In this case, the interval error of the pattern would cause an error in Y_T. As a solution to this error, a mean value of four patterns was used, and this proved the feasibility of the measured system.

4. Conclusions

The conventional measurement methods for obtaining the effective focal length, such as the nodal slide and magnification methods, are not useful for center-obstructed omni-directional optical systems. Therefore, the focal length of a center-obstructed omni-directional reflective optical system with an FOV of 80–135° was measured by applying the novel measurement method described in this paper. The EFL calculated using the measurements from our proposed measurement system was 0.3739 mm, which was only ~11 μm from the EFL obtained using the design software. In addition, the tolerance was calculated and compared with the theoretical value obtained for the omni-directional optical system to verify the validity of the measurement method. By applying the tolerance level commonly used in practice to the optical system, we concluded that the measured EFL falls within the tolerance range of ±15 μm. The measurement reliability could be increased if the sources of measurement error mentioned in this paper were reduced.

Supplementary Materials: Supplementary materials are available online http://www.mdpi.com/2076-3417/9/11/2350/s1. Table S1: Specifications of our designed omni-directional optical system; Table S2: Number of pixels for each zone and real ray heights on the sensor; Table S3: Measured and theoretical values; Table S4: The calculated focal lengths; Table S5: Focal length sensitivity for tolerance; Table S6: Permissible errors for focal length (in mm).

Author Contributions: Conceptualization, H.C., J.-M.R.; methodology, J.-Y.J., J.-M.R.; software, J.-Y.J., J.-M.R.; validation, J.-M.R.; data curation, J.-Y.J., J.-M.R.; writing—original draft, H.C., J.-Y.J., J.-M.R.; supervision, J.-M.R.; funding acquisition, J.-M.R.

Funding: This research was supported by the Basic Science Research Program through the National Research Foundation of Korea (NRF) funded by the Ministry of Education (No. NRF-2017R1D1A3B03029119).

Acknowledgments: The authors thank the Editing Service for editing the English of this scientific paper.

Conflicts of Interest: The authors declare no conflict of interest.

References

1. Kruegle, H. *CCTV Surveillance: Video Practices and Technology*; Elsevier: Amsterdam, The Netherlands, 2011.
2. Javidi, B. *Optical and Digital Techniques for Information Security*; Springer Science & Business Media: Berlin, Germany, 2006; Volume 1.
3. Clark, A.D.; Wright, W. *Zoom Lenses*; Adam Hilger Ltd.: London, UK, 1973.
4. Choi, H.; Ryu, J.; Kim, J. A novel fisheye-lens-based photoacoustic system. *Sensors* **2016**, *16*, 2185. [CrossRef]
5. Popovic, V.; Seyid, K.; Cogal, Ö.; Akin, A.; Leblebici, Y. State-of-the-art multi-camera systems. In *Design and Implementation of Real-Time Multi-Sensor Vision Systems*; Springer: New York, NY, USA, 2017; pp. 13–31.
6. Russ, J.C. *The Image Processing Handbook*; CRC Press: Boca Raton, FL, USA, 2016.
7. Malacara-Hernández, D.; Malacara-Hernández, Z. *Handbook of Optical Design*; CRC Press: Boca Raton, FL, USA, 2016.
8. Jo, J.H.; Lee, S.; Seo, H.J.; Lee, J.H.; Kim, J.M. Design of omnidirectional camera lens system with catadioptic system. In Proceedings of the SPIE Optical Metrology—International Society for Optics and Photonics, Munich, Germany, 13–16 May 2013; p. 87882Q.
9. Japanese Standards Association. *JIS Handbook 2013*; Japanese Standards Association: Tokyo, Japan, 2013.
10. Chaves, J. *Introduction to Nonimaging Optics*; CRC Press: Boca Raton, FL, USA, 2008.
11. Choi, H.; Yeom, J.-Y.; Ryu, J.-M. Development of a multiwavelength visible-range-supported opto–ultrasound instrument using a light-emitting diode and ultrasound transducer. *Sensors* **2018**, *18*, 3324. [CrossRef] [PubMed]
12. Choi, H.; Ryu, J.-M.; Yeom, J.-Y. Development of a double-gauss lens based setup for optoacoustic applications. *Sensors* **2017**, *17*, 496. [CrossRef] [PubMed]
13. Smith, W.J. *Modern Optical Engineering*; McGraw-Hill Education: New York, NY, USA, 2007.
14. Kingslake, R.; Johnson, R.B. *Lens Design Fundamentals*; Academic Press: Cambridge, MA, USA, 2009.
15. Little, R.J.; Rubin, D.B. *Statistical Analysis with Missing Data*; John Wiley & Sons: Hoboken, NJ, USA, 2014.
16. Smith, W.J. *Modern Lens Design*; McGraw-Hill: New York, NY, USA, 2005.

17. Ryu, J.M.; Kim, Y.S.; Jo, J.H.; Kang, G.M.; Lee, H.J.; Lee, H.K. Statistical analysis of focus adjustment method for a floating imaging system with symmetric error factors. *Korean J. Opt. Photonics* **2012**, *23*, 189–196. [CrossRef]
18. Mendenhall, W.; Beaver, R.J.; Beaver, B.M. *Introduction to Probability and Statistics*; Cengage Learning: Boston, MA, USA, 2012.
19. Ryu, J.; Jo, J.; Kang, G.; Lee, H.; Yoneyama, S. Focus adjustment method with statistical analysis for an interchangeable zoom lens with symmetric error factors. *Korean J. Opt. Photonics* **2011**, *22*, 230–238. [CrossRef]
20. Dainty, J.C. *Laser Speckle and Related Phenomena*; Springer Science & Business Media: Berlin, Germany, 2013.
21. Montgomery, D.C. *Introduction to Statistical Quality Control*; John Wiley & Sons: Hoboken, NJ, USA, 2007.

© 2019 by the authors. Licensee MDPI, Basel, Switzerland. This article is an open access article distributed under the terms and conditions of the Creative Commons Attribution (CC BY) license (http://creativecommons.org/licenses/by/4.0/).